

# WTrack: HMM-based walk pattern recognition and indoor pedestrian tracking using phone inertial sensors

Xiaoguang Niu · Meng Li · Xiaohui Cui ·  
Jin Liu · Shubo Liu · Kaushik R. Chowdhury

Received: 18 February 2014 / Accepted: 29 April 2014 / Published online: 9 August 2014  
© Springer-Verlag London 2014

**Abstract** Indoor tracking systems have become very popular, wherein pedestrian movement is analyzed in a variety of commercial and secure spaces. The inertial sensor-based method makes great contributions to continuous and seamless indoor pedestrian tracking. However, such a system is vulnerable to the cumulative locating errors when moving distance increases. Inaccurate heading values caused by the interference of body swing of natural walking and the geomagnetic disturbances are the main sources of the accumulative errors. To reduce such errors, additional infrastructure or highly accurate sensors have been used by previous works that considerably raise the complexity of the architecture. This paper presents an

indoor pedestrian tracking system called WTrack, using only geomagnetic sensors and acceleration sensors that are commonly carried by smartphones. A fine-grained walk pattern of indoor pedestrians is modeled through Hidden Markov Model. With this model, WTrack can track indoor pedestrians by continuously recognizing the pre-defined pedestrians' walk pattern. More importantly, WTrack is able to resist both the interference of body swing of natural walking and the geomagnetic disturbances of nearby objects. Our experimental results reveal that the location error is  $<2$  m, which is considered adequate for indoor location-based-service applications. The adaptive sample rate adjustment mode further reduces the energy consumption by 52 % in comparison, as opposed to the constant sampling mode.

---

X. Niu · M. Li · J. Liu (✉) · S. Liu  
Computer School, Wuhan University, Wuhan, China  
e-mail: mailjinliu@yahoo.com

X. Niu  
e-mail: xgniu@whu.edu.cn

M. Li  
e-mail: cslimeng@whu.edu.cn

S. Liu  
e-mail: sliu@whu.edu.cn

X. Cui (✉)  
International School of Software, Wuhan University, Wuhan,  
China  
e-mail: cuixhui@gmail.com

J. Liu  
State Key Lab of Software Engineering, Wuhan University,  
Wuhan, China

K. R. Chowdhury  
Department of Electrical and Computer Engineering,  
Northeastern University, Boston, MA, USA  
e-mail: krc@ece.neu.edu

**Keywords** Indoor pedestrian tracking · Walk pattern recognition · Smartphone · Inertial sensing · Ubiquitous computing

## 1 Introduction

Indoor pedestrian tracking is an important enabling technology in many indoor establishments, such as restaurants, supermarkets, and parking lots. In such environments, it is very important to collect pedestrians' tracking information for physical behavior analysis that has many QoS, traffic estimation, and security applications [1]. With the widespread use of smartphones, indoor pedestrian tracking system using the sensors available on the smartphone has seen a lot of research interest in recent years [2, 3].

Indoor pedestrian tracking technologies can be classified into two general methods: location fingerprinting-based method [4, 5] and inertial sensor-based approach [6, 7].

Location fingerprinting-based tracking technologies cover a large range and possess higher precision, which are suitable for long-time positioning. However, it is unable to realize continuous and seamless tracking due to the problem of blind spots in coverage. Additionally, the fingerprinting scheme requires a costly process of radio map construction based on AP infrastructure. Inertial sensors positioning is widely used to track a pedestrian by continuously estimating displacement from an unknown location [8]. The so-called pedestrian navigation system (PNS) is an instance of such a dead reckoning approach. The inertial sensor-based method makes great contributions to continuous and seamless indoor localization and does not require any additional infrastructure requirement. However, due to its hardware characteristics, this method is vulnerable to the accumulation of errors from sensor readings when moving distance increases, and inaccurate heading values captured from the geomagnetic sensor are the main sources of the accumulative error [9, 10]. The factors of inaccurate heading can be divided into two main aspects: the geomagnetic disturbances and the body swing. As the tracking accuracy depends critically on the sensors data, the accumulation of errors should not be compromised by the designer of indoor pedestrian tracking system.

To address the inherent problem of cumulative location errors, many previous works have tried to limit the usage of sensors or the tracking area, such as constraining the sensor placement to a certain position in order to obtain a correct sensor reading [11, 12]. These systems are usually applicable part of the indoor environment and obviously not practical in real indoor environment. There are other schemes that use highly accurate sensors to handle this inherent problem [13]. These schemes can improve the tracking accuracy, while they require additional costs owing to their high precision or the need of auxiliary positioning devices, apart from the physical discomfort of the subject owing to direct body contact.

Recently, the approach of Hidden Markov Model (HMM) has become a useful tool in the research community for modeling spatiotemporal variability and feature extraction. In this paper, we proposed WTrack, an indoor pedestrian tracking system, which is applicable to various indoor environments. This system is capable of handling noisy sensors including body swing of natural walking and geomagnetic disturbances without any additional infrastructure, and provides a meter-level positioning accuracy for users with common smartphone devices. To summarize, the contributions of our work include:

- We built an indoor pedestrian tracking system using only geomagnetic sensors and acceleration sensors that are commonly carried by smartphones, in which the

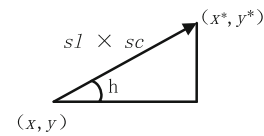


**Fig. 1** Principle of dead reckoning

algorithm can recognize and calibrate the geomagnetic disturbances caused by objects.

- With the pre-defined fine-grained walk pattern, we developed HMM-based walk pattern recognition to track indoor pedestrians, which is robust to body swing of natural walking. Outlier and bad zone of the trace can be recognized and calibrated.
- To capture accurate sensor data with minimum energy consumption, we propose an adaptive sampling mode, which allows the sensors to change their sampling rates according to the walking states of pedestrians.

The remainder of the paper is organized as follows: Sect. 2 discusses the challenges of the pedestrian tracking in indoor environments. The components and design contributions of the proposed WTrack scheme are described in detail in Sect. 3. Then, we present the experimental results and evaluate the performance of WTrack in Sect. 4. Section 5 discusses the related works in indoor pedestrian systems. Finally, Sect. 6 concludes the paper.

## 2 Challenges and motivation

### 2.1 Overview of inertial sensors-based tracking system

In the following discussion, indoor pedestrian tracking systems use only geomagnetic sensors and acceleration sensors presented in smartphones to collect information about the pedestrian's location, along with the heading and distance moved. Then, we can get pedestrian's trace by the method of dead reckoning with the collected sensor data.

The displacement and heading for walking are obtained by the above sensors. Then, the pedestrian's position can be calculated using the method of dead reckoning, as shown in Fig. 1. The initial location of the pedestrian can be denoted as  $(x, y)$ . The step length and step count are denoted as  $sl$  and  $sc$ , respectively. The step length and step count estimate process is out of scope of this paper.  $h$  represents the heading captured from geomagnetic sensor. Then, traces of indoor pedestrians can be obtained by continuous calculation with the following formula:

$$(x^*, y^*) = (x + sl \times sc \times \cos h, y + sl \times sc \times \sin h)$$

In particular, we will focus on how to achieve an accurate heading value from the geomagnetic sensor in this paper.

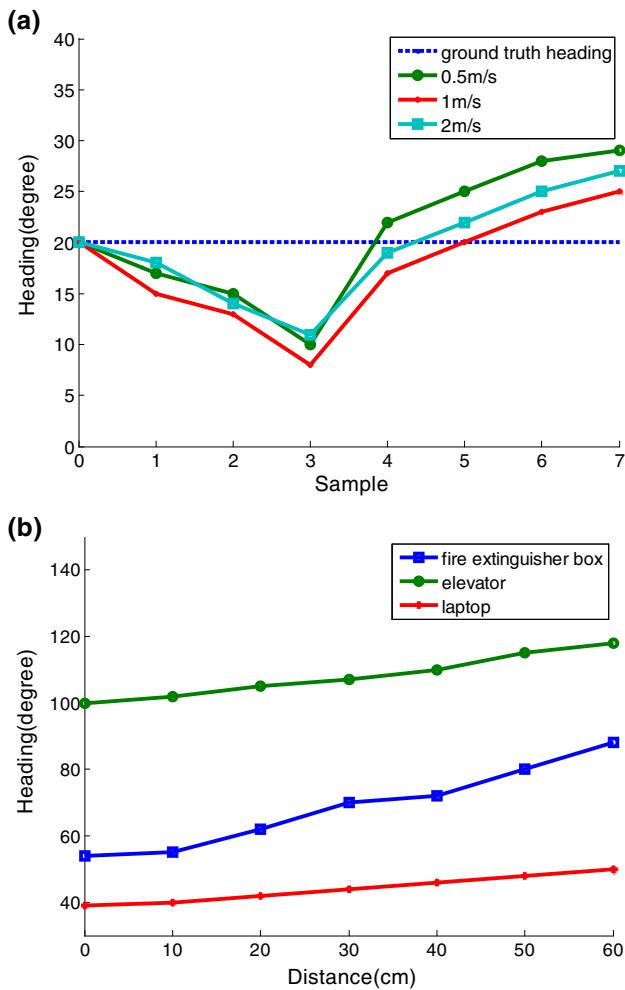


**Fig. 2** Influences of body swing of natural walking and geomagnetic disturbances. **a** Heading with body swing and the ground truth heading in one step at different speed. **b** Heading with geomagnetic disturbances for three objects

### 2.2 Challenges

A pedestrian tracking system with smartphone relies on acquiring an accurate heading from the geomagnetic sensor in order to produce reliable displacement estimation. Inaccurate heading values are the main sources of the accumulative error which is a nontrivial task for indoor tracking system. The geomagnetic sensor reading can be affected by many factors in real indoor environments. Generally, the factors of inaccurate heading value can be divided into two aspects: the body swing of natural walking and the geomagnetic disturbances.

The error originated in body swing is an important part of the overall error seen in the tracking process. As we all know, body swing is natural and inevitable when a pedestrian normally walks. Obviously, such body swings will lead to the shaking of smartphones held in hands, and the sensor data collected from the geomagnetic sensor will

**Table 1** The impact on ground truth heading caused by different objects

Objects	Ground truth heading (°)
Elevator	130
Fire extinguisher box	90
Laptop	68

be constantly changing during one step. We have done a quantitative experiment to describe it, as shown in Fig. 2a. The ground truth heading of a pedestrian is 20°. Nevertheless, the collected seven heading samples in one step deviate from the ground truth heading to varying degrees due to the influence of body swing, and the deviation is associated with the walking speed of the pedestrian. Therefore, in most cases, heading collected at a particular moment of one step cannot fully represent the heading of this whole step. A reasonable walking model should be established to resist the interference of body swing of natural walking.

Compared to the body swing of natural walking, geomagnetic disturbances caused by nearby objects have a significantly higher impact on heading values. To examine the effects of nearby objects, we select several different objects such as an elevator, a laptop (DELL vostro5460), and fire extinguisher box. Then, we fix the objects location and measure the heading value collected from geomagnetic sensor as the sensor is brought closer to the objects. For comparison purposes, we did this both with and without these objects, and the test without these objects is considered to the ground truth of the heading value, as shown in Table 1. By comparing the actual collected heading value in Fig. 2b with the ground truth heading, we find that the influence from these objects rises quickly as the distance decreases in the case of interference from some objects. When the distance is <10 cm, the influence is nearly double the ground truth which is obviously out of the tolerance of indoor pedestrian tracking system. Therefore, the effect of geomagnetic disturbances should be compromised by the system designer when providing meter-level positioning accuracy for common smartphone users. Additionally, it is difficult to predict and identify these geomagnetic disturbances with traditional approaches, because the effect of different objects is hard to quantize or model.

Furthermore, as we cannot simply judge whether a position point is right or not from its macro-position in the trace, because in some cases, some wrong points in the whole traces seem to be reasonable if judging from the macro-perspectives. Thus, a novel micro-perspective methodology which focuses on the observation within one step needs to be designed.

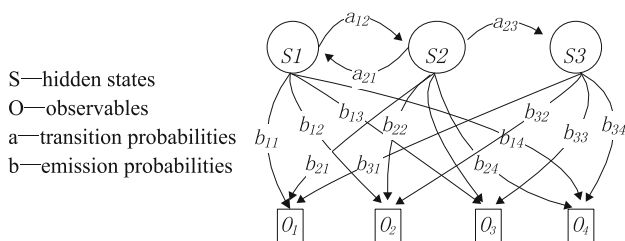


Fig. 3 Structure of HMM

### 3 WTrack: HMM-based walk pattern recognition and pedestrian tracking

Aimed at reducing the cumulative locating errors that are caused by noisy inertial sensors in dead reckoning systems, we propose a HMM-based fine-grained walk pattern recognition and pedestrian tracking system, called WTrack. WTrack firstly defines walk patterns for indoor pedestrians and models them with HMM. Then, this system tracks indoor pedestrians by continuously recognizing the pre-defined walk pattern of the pedestrian.

#### 3.1 Hidden Markov Model

The Hidden Markov Model focuses on analyzing correlation of spatiotemporal information and modeling them mathematically. Related to HMM, there are several efficient algorithms for learning and recognition, such as the Baum-Welch algorithm [14] and Viterbi algorithm [15]. Figure 3 shows the structure of HMM, where a collection of states is connected by transitions. Each transition has a pair of probabilities: a transition probability (which provides the probability for undertaking the transition) and an emission probability (which defines the conditional probability of emitting an output symbol from a finite alphabet, given a state). A formal characterization of HMM is shown as:

$\{s_1, s_2, s_3, \dots, s_N\}$ —A set of  $N$  hidden states. The state at time  $t$  is denoted by the random variable  $q_t$ .

$\{v_1, v_2, v_3, \dots, v_M\}$ —A set of  $M$  distinct observations. The observation at time  $t$  is denoted by the random variable  $O_t$ . The observations correspond to the physical output of the system being modeled.

$A = [a_{ij}]$ —An  $N \times N$  matrix for the state transition probability distributions, where  $a_{ij}$  is the probability of making a transition from state  $s_i$  to  $s_j$ :

$$a_{ij} = P(q_{t+1} = s_j | q_t = s_i).$$

$B = [b_j(i)]$ — $b_j(i)$  is output probability at time  $t$  in state  $s_j$ :

$$b_j(i) = P(o_t = v_i | q_t = s_j).$$

$\pi = [\pi_i]$ —The initial state distribution, where  $\pi_i$  is the probability that the state  $s_i$  is the initial state:

$$\pi_i = P(q_1 = s_i).$$

We use the compact notation  $\lambda = (A, B, \pi)$  to represent an HMM. The specification of an HMM involves the choice of the number of states  $N$ , and the number of discrete symbols  $M$ , and the specification of the three probability densities  $A$ ,  $B$ , and  $\pi$ .

#### 3.2 HMM-based fine-grained walk pattern recognition

To cope with the accumulative errors caused by body swing of natural walking in indoor pedestrian tracking, we model walk patterns during walking for pedestrian with HMM referring to the characteristics of indoor pedestrian. In our case, the hidden states correspond to walk patterns. While the output (list of observations of indoor pedestrians) is known, the sequence of hidden states (walk patterns of indoor pedestrians) is not. Our goal is to measure the probability for each type of walk pattern and recognize the most likely walk pattern of the pedestrian.

Prior to using an HMM, we first need to define the appropriate walk pattern in our system which actually corresponds to the hidden states of HMM and select the representative observations for it.

##### 3.2.1 Walk pattern

We classify walk patterns of indoor pedestrians with heading and speed. Figure 4 shows the definition of walk pattern. In order to facilitate the analysis, we divide the  $360^\circ$  of a circle into 24 heading segments with the intervals of  $15^\circ$ . Then, the heading of the pedestrians can be classified as one of the 24 heading segments. On the other hand, considering that normal speed range of indoor pedestrians is 0.5–2 m/s, we classify the speed of indoor pedestrians into three speed types: slow (with the speed range of 0.5–1 m/s), medium (with the speed range of 1–1.5 m/s), and fast (with the speed range of 1.5–2 m/s). Hence, walk patterns of indoor pedestrians can be divided into a total of 72 types, every walk pattern contains two aspects, heading segment and speed type. For a given heading and speed, walk patterns  $\{s_1, s_2, s_3, \dots, s_n\}$  can be expressed as:

$$s_i = (\text{heading segment}, \text{speed type}), \quad i = 1, 2, \dots, N$$

$$\text{where heading segment} = \frac{\text{heading}}{15^\circ},$$

$$\text{speed type} = \begin{cases} \text{slow} & 0.5\text{m/s} < \text{speed} < 1\text{m/s} \\ \text{media} & 1\text{m/s} < \text{speed} < 1.5\text{m/s} \\ \text{fast} & 1.5\text{m/s} < \text{speed} < 2\text{m/s} \end{cases}$$

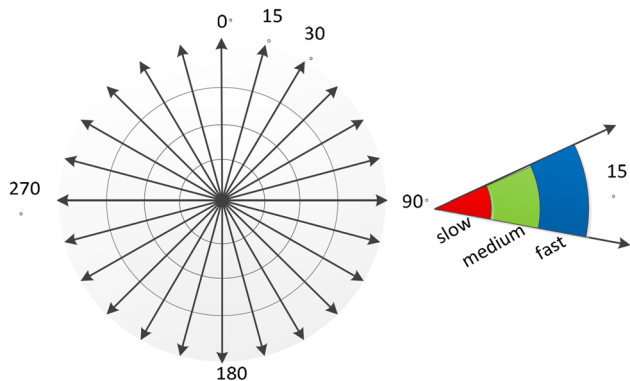


Fig. 4 Definition of walk pattern for HMM in WTrack

### 3.2.2 Observations

In order to highlight the distinction, three variables (i.e., the variation of the heading  $\Delta hd$ , the  $z$ -axis acceleration  $acce$  and the walking speed  $spd$ ) are selected as the observations to reflect the fine-grained characteristics of the indoor walk pattern in one step. To facilitate measuring, we divide the walking time of one step  $T$  into  $N$  equal portions, which returns the time for the collecting sensor data  $t_n$  as  $nT/N$ ,  $n = 1, 2, \dots, N$ . At each  $t_n$ ,  $n = 1, 2, \dots, N$ , we collect data from inertial sensors as observation  $O_i = (\Delta hd_i, acce_i, spd_i)$ ,  $i = 1, 2, \dots, N$ . Then, the observations of HMM  $v_i$  can be expressed as:

$$v_i = [O_1, O_2, \dots, O_N]$$

**3.2.2.1 The variation of heading** To reflect the trend of heading within one step, we select the variation of the heading as one of the observations. According to established human walking statistics, the time range of normal walking is 0.2–2 s. We define that the corresponding heading at time  $t_i$  is  $hd_i$ ,  $i = 1, 2, \dots, N$ . The variation of heading  $\Delta hd_i$  at time  $t_i$  can be expressed as:

$$\Delta hd_i = hd_i - hd_{i-1}, \quad i = 1, 2, \dots, N$$

**3.2.2.2 Z-axis acceleration** Z-axis acceleration captured from acceleration sensor reflects pedestrian’s acceleration in the vertical direction. In order to identify the distortion caused by the body swing of natural walking, we select the  $z$ -axis acceleration as one of the observations.  $acce_i$  is the  $z$ -axis acceleration at time  $t_i$  ( $i = 1, 2, \dots, N$ ).

**3.2.2.3 Speed** In normal walking process, speed during each step is relatively stable and easy to distinguish due to personal walking habits, so speed is the important auxiliary observations to recognize walk. The speed of each step can be obtained by integrating the instantaneous acceleration at each step of the pedestrians.

### 3.2.3 Transition probabilities

Transitions among the hidden states are governed by a different set of probabilities called transition probabilities. Our transition probabilities reflect the following three notions: (1) In general, there is a higher probability that the walking pedestrians keep the preceding walk pattern, instead of changing their walking directions or speeds frequently. (2) Pedestrians can only change the walk pattern from the end of one step to the start of the next, if the person walks continuously and normally, i.e., a pedestrian cannot change the walk pattern in one step, which ensures that the walk pattern of pedestrians within one step is stable and without change. (3) A pedestrian cannot walk unreasonably fast in any walk pattern.

The transition probability  $p$  from the walk pattern  $i$  to the walk pattern  $j$  is set as follows. We divide the transition probability  $p$  into two components that are the transition probability of heading  $P_{\text{heading}}$  and the transition probability of speed  $P_{\text{speed}}$ . So, the transition probability distribution matrix ( $A$ ) of HMM can be expressed as:

$$A = \begin{pmatrix} a_{11} & \dots & a_{1j} \\ \vdots & \ddots & \vdots \\ a_{i1} & \dots & a_{ij} \end{pmatrix}, a_{ij} = P_{\text{heading}}(i, j) \times P_{\text{speed}}(i, j)$$

The transition probability of heading  $P_{\text{heading}}(i, j)$  from hidden state  $i$  to hidden state  $j$  is set as follows: We define  $P_{\text{heading}}(i, j) = \theta/2^n$ , where  $n = |i_{\text{heading}} - j_{\text{heading}}|$ ;  $i_{\text{heading}}$  and  $j_{\text{heading}}$  are the heading segment that heading of  $i$  and  $j$  are belonged to, respectively.  $\theta$  is the transition probability of heading when  $j$  keep the same heading segment with  $i$ , and  $\theta$  is the highest transition probability of heading from hidden state  $i$  to hidden state  $j$  which reflects the first notion. Note that  $P_{\text{heading}}(i, j)$  must satisfy the constraints:

$$\sum_{j=1}^k P_{\text{heading}}(i, j) = 1$$

where  $k$  represents total types of hidden states.

The transition probability of speed  $P_{\text{speed}}(i, j)$  can be calculated as follows.  $i_{\text{speed}}$  and  $j_{\text{speed}}$  are speed type that speed of hidden state  $i$  and hidden state  $j$  are belonged to, respectively.  $\omega$  is the transition probability of speed when  $j$  keep the same speed type with  $i$ , and  $\omega$  is the highest transition probability of speed from state  $i$  to states  $j$ , which also reflects the first notion. We define the transition probability of speed as:

$$P_{\text{speed}}(i, j) = \frac{\omega}{2^n}, n = |i_{\text{speed}} - j_{\text{speed}}|$$

By the same token,  $P_{\text{speed}}(i, j)$  must satisfy the constraints:

$$\sum_{j=1}^k P_{\text{speed}}(i, j) = 1$$

where  $k$  represents total types of hidden states.

### 3.2.4 Ground truth

To recognize the most likely walk pattern, we must choose the appropriate ground truth or the reference signature pattern. Obtaining this ground truth is a fundamental challenge in the recognition of walk patterns, we use an approach based on aggressive data cleaning to produce this ground truth with reasonable confidence for a set of indoor walk pattern.

We preprocess the data to obtain a standardized walk pattern by setting up a standard fingerprint database for each walk pattern. This is actually a sequence of <walk pattern, observations> pairs. For each walk pattern, participants walk with mobile phones in the corresponding walk pattern and record the standard observations, which are along the three metrics defined above (the variation of heading, z-axis acceleration, and speed). This trial is repeated many times in different indoor areas, using different mobile phones, as well as choosing different participants. Then, the average of all the collected measurements serves as the final fingerprint data. To ensure the credibility of the fingerprint database, we clean the output data to satisfy the following constraints: No walk time of one step exceeds 2 s, each heading value of one step is matched to heading segment at most  $10^\circ$  from it, and z-axis acceleration of pedestrians is  $<15 \text{ m/s}^2$  but more than  $0 \text{ m/s}^2$ . It is believed that these constraints taken together define a signature set of standard observations that can be treated as ground truth with high confidence.

### 3.2.5 Walk pattern recognition

The emission probabilities in WTrack reflect the notion that every walk pattern emits an observation with a particular conditional probability distribution. Concretely, the emission probability density of hidden state  $s_j$  with observations  $v_i$  is described as follows:

Given the walk pattern  $s_j$ , the standard observations  $v_j = [O_1^*, O_2^*, \dots, O_N^*]$  can be obtained by querying <walk pattern, observations> pairs of standard fingerprint databases. Observations of HMM  $v_i$  can be expressed as  $v_i = [O_1, O_2, \dots, O_N]$ . For observation  $v_i$  and standard observations  $v_j$ , each observation component  $O_n$  and  $O_n^*$  ( $n = 1, 2, \dots, N$ ) is a three-dimensional vector including variation of the heading  $\Delta hd_i$ , the z-axis acceleration  $acce_i$ , and the walking speed  $spd_i$ :

$$O_n = (acce_n, \Delta hd_n, spd_n),$$

$$O_n^* = (acce_n^*, \Delta hd_n^*, spd_n^*), \quad n = 1, 2, \dots, N$$

Here, we take the Euclidean distance between two vectors of observations to measure the difference between the actual observations and the standard observations. The Euclidean distance  $\text{dis}(O_n, O_n^*)$  between  $O_n$  and  $O_n^*$  is

$$\text{dis}(O_n, O_n^*) = \sqrt{(acce_n - acce_n^*)^2 + (\Delta hd_n - \Delta hd_n^*)^2 + (spd_n - spd_n^*)^2}$$

Then, the Euclidean distance  $\text{dis}(v_i, v_j)$  between actual observation  $v_i$  and standard observation  $v_j$  is:

$$\text{dis}(v_k, v_j) = \sqrt{\sum_{n=1}^N \text{dis}(O_n, O_n^*)^2}$$

$$= \sqrt{\sum_{n=1}^N (acce_n - acce_n^*)^2 + (\Delta hd_n - \Delta hd_n^*)^2 + (spd_n - spd_n^*)^2}$$

Hence, the emission probability density  $B = \{b_j(i)\}$  of hidden state  $s_j$  with the observations  $v_i$  is:

$$B = [b_j(i)] = \begin{pmatrix} b_{11} & \dots & b_{1j} \\ \vdots & \ddots & \vdots \\ b_{i1} & \dots & b_{ij} \end{pmatrix},$$

$$b_{ij} = p(o_t = v_i | q_t = s_j) = g(\text{dis}(v_i, v_j)) = e^{-\frac{\text{dis}(v_i - v_j)^2}{2\sigma^2}}$$

where  $g(x)$  is the Gaussian function with zero mean. The variance of  $g(x)$  depends on the sensor that produced the observations. To this point, we have accomplished to model walk pattern of indoor pedestrians through HMM.

In the next stage, Viterbi decoding is used to recognize the maximum likelihood sequence of hidden states given a set of observables and the emission probability distribution matrix  $B$  and transition probability matrix  $A$ . This corresponds to the most likely sequence of walk patterns, given a sequence of observations. To find the single best state sequence  $Q = q_1 q_2 \dots q_t$  for the given observation  $O = O_1 O_2 \dots O_t$ , the quantity for Viterbi decoding is defined as:

$$\delta_t(i) \cong \max_Q P(Q, q_t = s_i, O | \lambda)$$

To get a single sequence of the walk pattern  $s_i$  with the highest output probability at time  $t$  and accounting for the first  $t$  observations, we use induction as follows:

$$\delta_1(j) = \pi_j b_j(O_1) \quad 1 \leq j \leq N$$

$$\delta_t(j) = \max_i (\delta_{t-1}(i) a_{ij} b_{iO_t}) \quad 2 \leq t \leq T, 1 \leq j \leq N$$

where  $a_{ij}$  represents the probabilities that the walk pattern transfers from  $i$  to  $j$  and  $b_{iO_t}$  is the probability of matching the walk pattern  $i$  to the observations  $O_t$ .

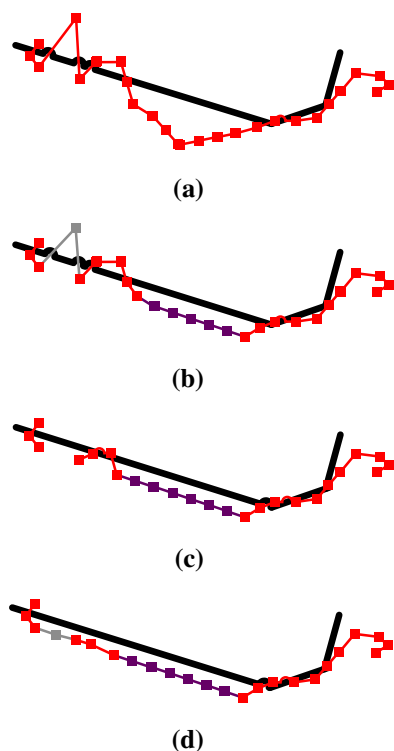


**Fig. 5** Indoor pedestrian tracking process. **a** Raw trace. **b** Walk pattern recognition. **c** Outlier removal. **d** Interpolation and bad zone calibration

For the backtracking information that is used to record the previous selection of a certain walk pattern that maximizes the local probability  $\delta_t(j)$  of for each  $t$  and  $j$ , we use a back pointer  $\psi_t(j)$ .

$$\psi_t(j) = \arg \max_i [\delta_{t-1}(i)a_{ij}] \quad 2 \leq t \leq T, 1 \leq j \leq N$$

In case of null transitions, the likelihood of the source state at time  $t$  is simply maximized without time delay as:

$$\delta_t(j) = \max_i [\delta_t(i)a_{ij}],$$

$$i^* = \operatorname{argmax}_i [\delta_t(i)a_{ij}],$$

$$\psi_t(j) = \psi_t(i^*)$$

For reliable walk pattern recognition, we define a constant threshold  $p$  (TH) for the output probability of Viterbi decoding algorithm  $\delta_t(i)$ . If  $\delta_t(i)$  is not less than the chosen threshold, the output walk pattern sequence is regarded legal and the walk pattern is recognized with high confidence.

Finally, to uncover the most likely state sequence  $Q^* = q_1^*q_2^* \dots q_T^*$  after the preceding computation, we must trace back to the initial state by following the Viterbi path of  $\psi_s$  as:

$$q_T^* = S_N,$$

$$q_t^* = \psi_{t+1}(q_{t+1}^*), \quad t = T - 1, T - 2, \dots, 1$$

$Q^* = q_1^*q_2^* \dots q_T^*$  is the final recognized walk pattern. Then, we extract the heading from the walk pattern to track the pedestrian. Figure 5 shows the indoor pedestrian tracking process. Figure 5a shows that raw trace of pedestrians (shown in red) calculated with the raw heading value collected in a random time of one step. As we can see, it greatly deviates from real traces (shown in black). Figure 5b shows the result of walk pattern recognition. Segments of the trace shown in purple are in close agreement with the real trace after tracking with the HMM-based walk pattern recognition.

### 3.3 Outlier removal and bad zone calibration

#### 3.3.1 Outlier removal

Point  $p$  is recognized as an outlier if it satisfies any of the following conditions:

- Heading calculation of  $p$  cannot match any heading segment of walk pattern of the standard fingerprint, which also means heading of  $p$  is disorganized.
- Speed of  $p$  is illegal, which means its speed is beyond normal speed range of indoor pedestrians (0.5–2 m/s).

To recognize and eliminate the outliers with the HMM-based walk pattern recognition result, we take the output probability  $\delta_t(j)$  of Viterbi decoding as a metric to measure the reliability of the point. Then, we set a probability constraint, through a threshold  $p$  (TH), for reliability metric. A sample is recognized as an outlier only if its reliability metric is less than  $p$  (TH), which means the observations of that sample cannot be matched to any of defined walk patterns.

Because outliers are usually several points of the track, we divide the whole track into short sequences of points with a sliding window of length  $k$ . The sliding window moves backward one unit every time. Assuming length of the whole track is  $T$ , the number of short sequences of points can be expressed as  $C = (T - k + 1)$ , and we calculate the quantity  $\delta_t(j)$  for each short sequence of points and measure credibility of  $\delta_t(j)$  with the defined threshold  $p$  (TH). Then, if  $\delta_t(i)$  is less than the chosen threshold, the selected short sequence of points of the track is recognized as the outlier that should be eliminated, shown in Fig. 5b in gray. Experimental results verified the fact that the chosen threshold is intentionally conservative and accommodates for the body swing of natural walking or the interference of some electromagnetic devices (see Section 4).

#### 3.3.2 Bad zone calibration

Here, we focus on removing the outlier points from the tracking, which would cause outages in the tracking

process. The outages cause their following samples to also be incorrectly mapped (called *bad zone*). The gray part in Fig. 5d shows the bad zone for an instance of tracking. Therefore, after outlier removal, a simple scheme is proposed to deal with outages and bad zone by inserting interpolated points in such regions. The bad zone is calibrated by exploiting the preceding normal observations through curve fitting method. The algorithm generates interpolated samples at 1 s intervals along the curve fitting direction of the track, connecting the last observed point before the outage, and the first following the outage, assuming a normal walking speed. Experimental results showed that this approach can match the interpolations to the outages of the track quite well and achieves good indoor positioning accuracy (see Sect. 4).

### 3.4 Geomagnetic disturbances recognition and calibration

We use three-axis accelerometer which is commonly carried by smartphones to recognize the geomagnetic disturbances caused by some nearby objects. We assume that an indoor pedestrian walk along a corridor with a smartphone, and turn at the corner. A geomagnetic disturbance source is placed in the middle of the corridor. For a particular step (denoted as step  $n$ ), we collect  $m$  acceleration samples of each axis, denotes as  $x_{n1}, x_{n2}, \dots, x_{nm}, y_{n1}, y_{n2}, \dots, y_{nm}$  and  $z_{n1}, z_{n2}, \dots, z_{nm}$ . Then, we measure RMS acceleration of them which can be calculated as follows:

$$\begin{aligned}
 xn &= \sqrt{\frac{x_{n1}^2 + x_{n2}^2 + \dots + x_{nm}^2}{m}}, \\
 yn &= \sqrt{\frac{y_{n1}^2 + y_{n2}^2 + \dots + y_{nm}^2}{m}}, \\
 zn &= \sqrt{\frac{z_{n1}^2 + z_{n2}^2 + \dots + z_{nm}^2}{m}}
 \end{aligned}$$

Thus, the feature acceleration of step  $n$  (denoted as  $\overline{acce}_n$ ) can be represented as a three-dimensional vector:  $\overline{acce}_n = (x_n, y_n, z_n)$

To judge whether the pedestrian turns or not, we compare the current step  $n$  with the previous two steps by calculating the Euclidean distance of three-axis acceleration between them, respectively, as:

$$\begin{aligned}
 \text{dis}(\overline{acce}_n, \overline{acce}_{n-1}) &= \sqrt{(x_n - x_{n-1})^2 + (y_n - y_{n-1})^2 + (z_n - z_{n-1})^2}, \\
 \text{dis}(\overline{acce}_n, \overline{acce}_{n-2}) &= \sqrt{(x_n - x_{n-2})^2 + (y_n - y_{n-2})^2 + (z_n - z_{n-2})^2}
 \end{aligned}$$

If  $\text{dis}(\overline{acce}_n, \overline{acce}_{n-1}) + \text{dis}(\overline{acce}_n, \overline{acce}_{n-2}) \leq \varepsilon$ , where  $\varepsilon$  represents the distance threshold, it indicates that the pedestrian walked straight in step  $n$ . Thus, if the heading

collected from the geomagnetic sensor changes significantly, it will be recognized as the geomagnetic disturbances. The pedestrian’s heading in step  $n$  will be calibrated to the walking heading in step  $n - 2$  (denoted as  $hd_{n-2}$ ). On the contrary, if  $\text{dis}(\overline{acce}_n, \overline{acce}_{n-1}) + \text{dis}(\overline{acce}_n, \overline{acce}_{n-2}) \leq \varepsilon$ , it indicates that the pedestrian turn at the corner in step  $n$ , and his heading should be determined by the heading value collected from the geomagnetic sensor (denoted as  $hd^*$ ). Therefore, the pedestrian’s heading (denoted as  $hd_n$ ) in step  $n$  can be described as:

$$\begin{aligned}
 &\text{If } n = 1 \text{ or } 2, hd_n = hd^*, \text{ else} \\
 hd_n &= \begin{cases} hd_{n-2} & \text{dis}(\overline{acce}_n, \overline{acce}_{n-1}) + \text{dis}(\overline{acce}_n, \overline{acce}_{n-2}) \leq \varepsilon \\ hd^* & \text{dis}(\overline{acce}_n, \overline{acce}_{n-1}) + \text{dis}(\overline{acce}_n, \overline{acce}_{n-2}) \geq \varepsilon \end{cases}
 \end{aligned}$$

### 3.5 Adaptive sample rate adjustment

To capture accurate sensor data with minimum energy consumption, the inertial sensors can adaptively change their sample rates according to the walking states of pedestrians. The adaptive sample rate adjustment is shown in Algorithm 1. The walking states of pedestrians are divided into two types: steady state and non-steady state. The heading values of pedestrians are used to measure walking states with  $h_d$  being the heading at time  $d$ . The input of this algorithm is a continuous heading value sequence  $h_i$  ( $i = 1, 2, k$ ). The variation of the heading  $h_d'$  reflects the change between two continuous heading samples. The variation of the heading change  $h_d''$  describes the variation between two continuous heading changes. When the pedestrian is walking straight or is in other stable states, heading value of pedestrians does not change sharply. Hence, the variation of the heading change  $h_d''$  is less than a certain minimum. The sample rate is set constant. Otherwise, when a pedestrian is always changing his walking state in some changeable indoor areas, it is likely a non-steady state. So sample rate, in this case, should be set to a higher one.

Algorithm1. Adaptive Sample Rate Adjustment
<b>Input:</b> a continuous heading values sequence $\{h_i, 1 \leq i \leq k\}$ , $d(3 \leq d \leq k)$ ;
<b>Output:</b> sample rate at $d^{th}$
<b>Procedure:</b>
1: calculate $h'_d = h_d - h_{d-1}$ ;
2: calculate $h'_{d-1} = h_{d-1} - h_{d-2}$ ;
3: calculate $h''_d = h'_d - h'_{d-1}$ ;
4: <b>if</b> $h''_d < \varepsilon$ ;
5: <b>then</b> low sample rate;
6: <b>else</b> high sample rate;
7: <b>end if</b>

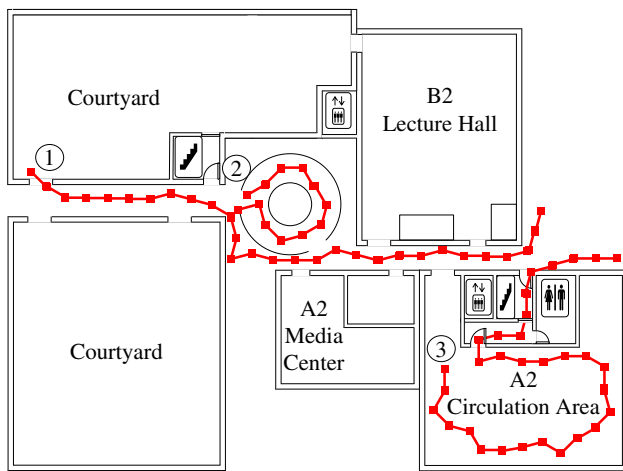


**Fig. 6** Three experimental routes in the New Library of Wuhan University

### 4 Performance evaluation

#### 4.1 Experimental setting

For the experimental study, we choose the second floor of the New Library of Wuhan University to evaluate the performance of WTrack system. Three representative areas in this place were selected for evaluating the performance of the system shown in Fig. 6: (1) a 20-m corridor between two courtyards, (2) an annular book reading area whose radius is 2.5 m, (3) a  $13.8 \times 9.9 \text{ m}^2$  circulation area, as shown in Fig. 6. This place includes some metal objects, such as elevators, which can disturb geomagnetic distribution and are common in indoor environment. We select three different smartphones (Samsung i9300, HTC T328 W and Lenovo K900) as the data collection tool, each of which is equipped with various sensor devices including acceleration sensors and geomagnetic sensors. During this experiment, we walked holding the mobile phone in the hand to continuously record the location, heading and three-axis acceleration. We have conducted extensive experiments on user with these smartphone devices, with over 50 subjects walking over an aggregate distance of over 40 km.

To select the appropriate threshold  $p$  (TH), we have counted errors and calculated the false-positive and false-negative rates by varying the threshold  $p$  (TH) for the output probability of Viterbi decoding algorithm  $\delta_i(i)$ . False-positive and false-negative rates for the walk pattern recognition for different threshold  $p$  (TH) are shown in Fig. 7. The result suggests that a high  $p$  (TH) may result in many normal samples being mistaken for outliers, so the false-positive rate improves. On the other hand, a low threshold  $p$  (TH) causes more outliers to be missed, so false-negative rate improves. Considering the studies on

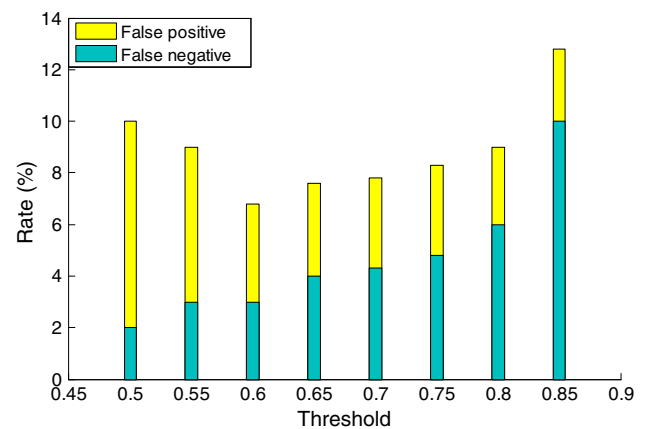


**Fig. 7** Threshold test for outlier recognition

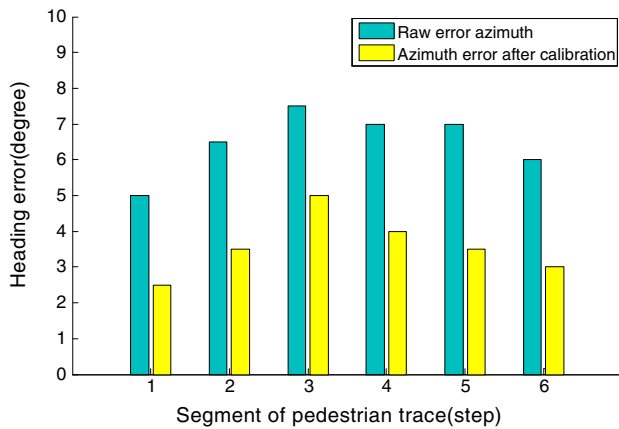
false-positive rate and false-negative rate comprehensively, we find that the best results are observed for  $p$  (TH) = 0.6.

#### 4.2 Heading correction

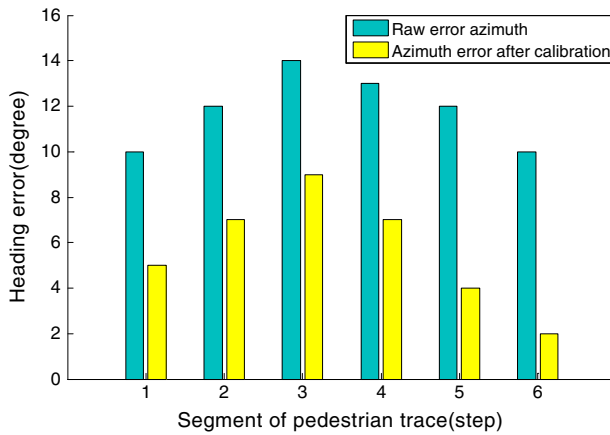
In tracking task, there are two types of noisy sensors: One type occurs due to the body swing of pedestrians' natural walking, and the other occurs when the captured heading is disturbed by various objects. Here, we explored the two types of noisy sensors by experimentation. We consider the heading error as the performance metric. This error can be calculated as: heading error = captured heading – actual heading

To explore the correction result for the body swing, we walked in the three representative areas and selected six steps in the typical segment of the area to calculate the heading error. Figure 8 shows heading error of the selected six steps, for raw heading error and heading error after calibration. The three figures describe heading error caused by body swing in three different areas. In Fig. 8a, the track is close to a straight line in the corridor, thus the heading of pedestrian only has small changes during the whole walking process. The heading error is minimal among the three areas. In contrast, for area 2, the track is nearly a circle which reflects that the heading of pedestrian is changing drastically during the whole walking process, as shown in Fig. 8b. Figure 8c shows that the heading error of area 3 is maximal of three tracks. Experimental results show that body swing has larger disturbances in heading calculation in the more complex areas than in straightforward arranged spaces. In additional, as we can see, the heading error after calibration reduces to nearly half of the raw heading error; 80 % of heading error after calibration is  $<15^\circ$  which is good enough for positioning.

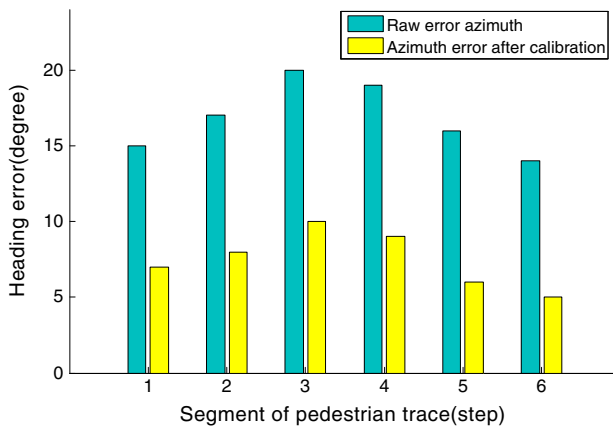
Next, to examine the interference of nearby objects, we select a representative trace in the experimental environment, as shown in Fig. 9. As we can see, there is an



(a)



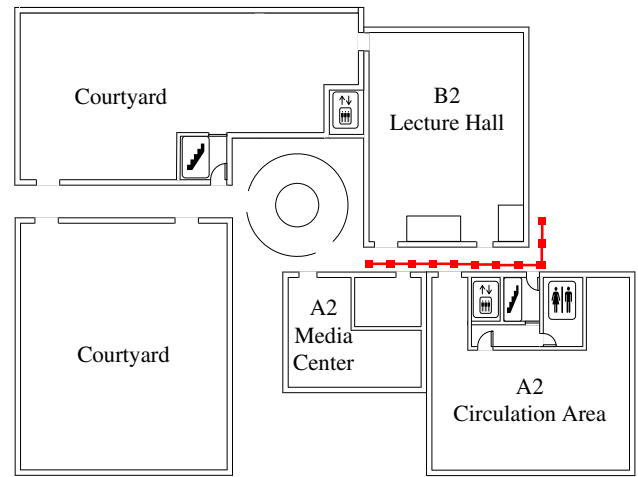
(b)



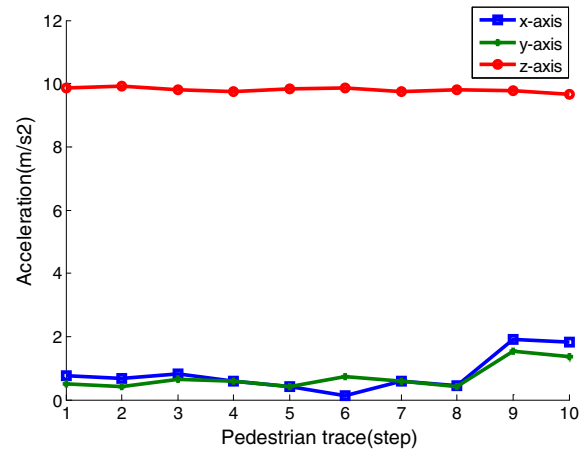
(c)

**Fig. 8** Correction results for body swing. **a** Area 1. **b** Area 2. **c** Area 3

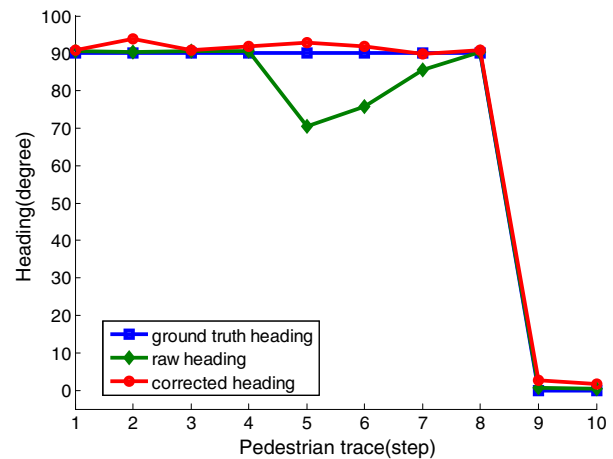
elevator near the path which is a common object in the indoor environment, and the distance between the elevator and pedestrian is 0.5 m. A participant walked ten steps holding the mobile phone in hands along the path for



(a)



(b)



(c)

**Fig. 9** Geomagnetic disturbances recognition and calibration test. **a** Selected path for geomagnetic disturbances test. **b** Three-axis acceleration of the pedestrian. **c** Heading calibration result

**Table 2** The results of geomagnetic disturbances recognition with different Euclidean distance threshold  $\varepsilon$

$\varepsilon$	False-positive rates (%)	False-negative rates (%)	Average error of the corrected heading (°)
0.5	2.4	7.5	9.12
1.0	3.1	7.1	7.25
1.5	3.5	6.5	6.54
2.0	3.9	5.2	5.56
2.5	4.4	5.0	8.21

several times. During the first eight steps, the participant walked straight to the east which indicates that participant’s actual heading is 90°. While the participant turns to the north at corner, the participant’s actual heading is 0° during the last two steps. We record the three-axis acceleration and the heading value of the participant, which is shown in Fig. 9b, c. In Fig. 9b, as the participant kept walking straight in the first eight steps, there is only a small fluctuation in the three-axis acceleration curve of the participant. But in the steps 9–10, when the participant turned at the corner, the  $x$ -axis and  $y$ -axis acceleration rises to nearly 2 m/s<sup>2</sup>. Compared with  $y$ -axis,  $x$ -axis acceleration witnessed a more obvious change when the participant turned. However, no matter the participant turned or walked straight, there are almost no significant changes of the  $z$ -axis acceleration from the beginning to the end. Heading value of the participant of the ten steps is shown in Fig. 9c with the default Euclidean distance threshold of 2.0. Comparing the ground truth heading with the raw heading, we can see that there is few heading error during the first four steps. But in steps 5–7, as the participant approaches the elevator, the raw heading drops quickly to <70° which denotes nearly 20° heading error because of the geomagnetic disturbances caused by the elevator. Nevertheless, if our method is applied, the heading is corrected to 90° immediately, which illustrates that our method can recognize the geomagnetic disturbances and calibrate the heading error effectively.

As we choose different threshold  $\varepsilon$  for the Euclidean distance of three-axis acceleration between step  $n$  and the previous step, the false-positive (FP), false-negative (FN) and the calibration results are shown in Table 2. Each of these values is a result based on testing 1,000 steps. We can see FP and FN rates increase for more strict thresholds (i.e., FP with a higher threshold or FN with a lower threshold). However, the overall FP and FN rates are still very slow, and the average error of the corrected heading is <10°. When  $\varepsilon$  is set to 2.0, the sum of FP and FN reaches to the minimum, and the average heading error also achieves the minimum value of 5.56° which is an acceptable error

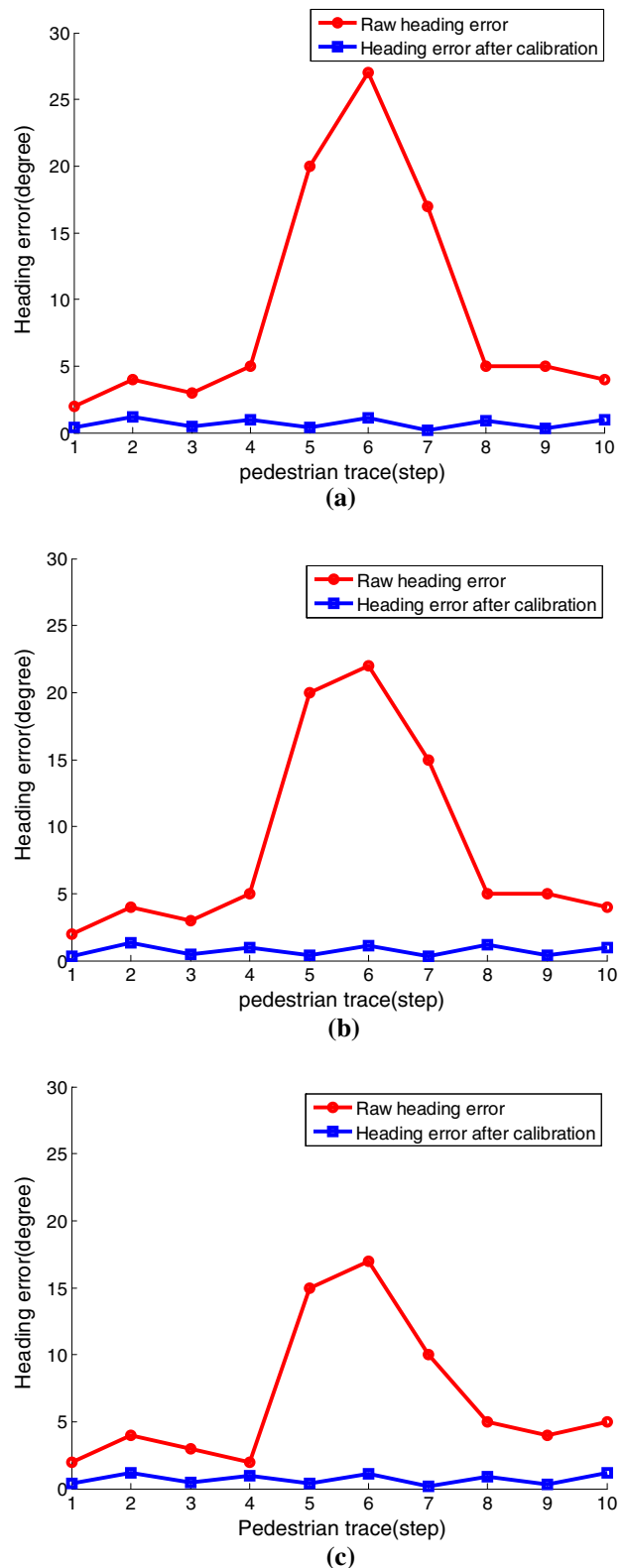


**Fig. 10** Heading correction results of geomagnetic disturbances test with different objects. **a** Geomagnetic disturbances test for fire extinguisher box. **b** Geomagnetic disturbances test for elevator. **c** Geomagnetic disturbances test for laptop

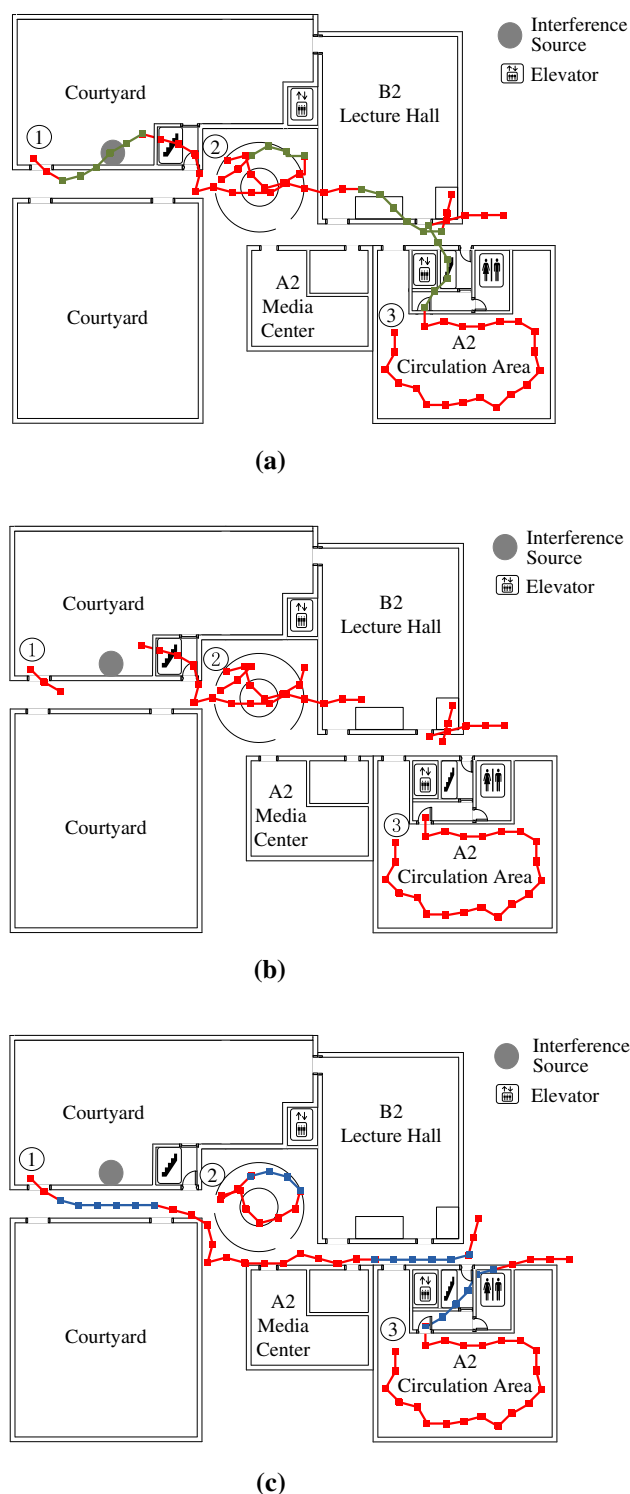


**Fig. 11** Pedestrian tracking results. **a** Raw track. **b** Outlier removal. **c** HMM-based tracking

range. There is a very minimal probability that we falsely recognize the geomagnetic disturbances, and the heading error is beyond  $5.56^\circ$ .

Figure 9 only shows the calibration result under the interference of elevator. As we have proved in Section 2,

different objects have varying degrees of impact on the heading value. Thus, we choose several different objects (i.e., fire extinguisher box, elevator, and laptop) to verify the heading correction result of our system, which is shown in Fig. 10.

As we can see, the heading in steps 5–7 is obviously disturbed by three objects. Once the participant comes close to the object in the sixth step, the heading error reaches to the top. Of all the three objects, fire extinguisher box has the most impact. However, once the heading is calibrated with our method, we can see that the heading error reduces significantly and the biggest heading error is  $<5^\circ$ . These results indicate that WTrack can effectively resist the geomagnetic disturbance caused by various objects and maintain the heading error of  $<5^\circ$ .

### 4.3 Tracking evaluation

A collection of indoor 50 tracks was collected in each area and preprocessed by filtering accidental data and taking average value of the remaining data. Figure 11a shows that the raw tracking is obviously distorted and cannot match the indoor map due to the interference source shown in green. The points in green are the recognized outliers which look like being “pulled” to the side close to the interference source. Once the raw tracking data are corrected with the recognized walk pattern, outliers are removed and interpolation applied, and the track curve becomes smooth and closer in shape to the actual track shown in Fig. 11b, c.

### 4.4 Positioning accuracy

Figure 12 shows the cumulative distribution function (CDF) of distance error introduced by the system for both 200 randomly selected 100-m-long tracks, for different types of indoor environment, as well as for different calibration methods. The distance error is a performance metric accuracy of a system as it represents the distance between ground truth track and the final track after calibration. It shows that there is about 20 % probability of the distance error of raw tracking being more than 4 m, which is beyond the tolerance limit for indoor positioning. Also, the distance error will accumulate as distance increases. Compared to the raw tracking, the WiFi auxiliary calibration gives 90 % chance of distance errorless being less than  $\sim 4$  m [17], but there is still a 20 % probability of it being more 4 m. In addition, Fig. 12 shows that the accuracy of HMM-based calibration is found to be within 2 m with the high probability of 92.5 %. Experimental results show WTrack can achieve a mean accuracy of 2 m in various indoor situations, which is considered adequate for indoor location-based service applications.

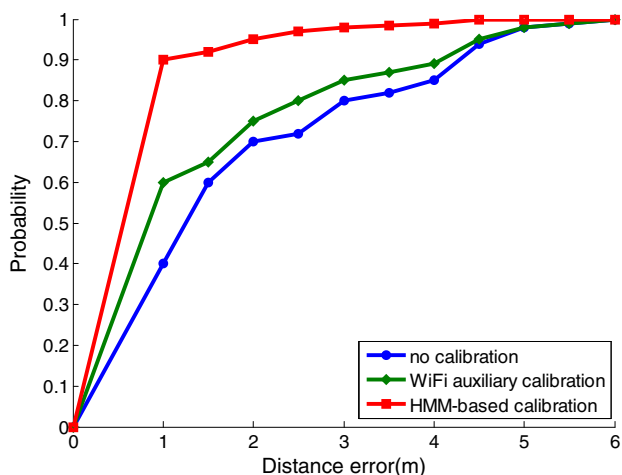
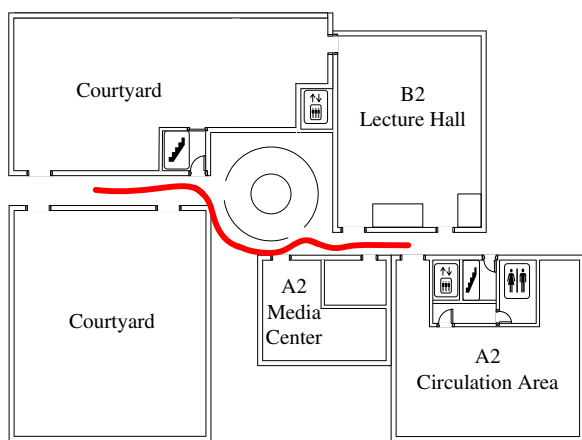
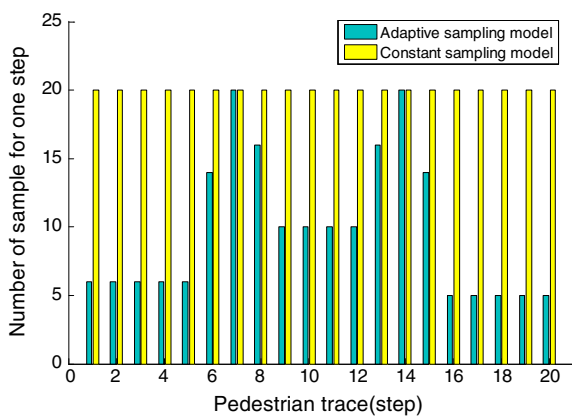


Fig. 12 CDF of distance error



(a)



(b)

Fig. 13 Energy efficiency using constant sampling mode and adaptive sampling mode. a Selected trace for energy efficiency experiments. b Number of sample for one step along a 10-m-long corridor

### 4.5 Energy efficiency

To get a better understanding of energy costs of this system on a smartphone, we measured the power consumption as an indicator. As the absolute power consumption of smartphones cannot represent the actual power consumption of our proposed approach due to background processes, we take the samples obtained in one step as the power consumption metric. A 10-m corridor on the second floor of the new library was chosen as the experiment site, shown in Fig. 13a. During this experiment, we run a simple application that repeatedly captures sensor data in the experimental site in constant sample rate mode and adaptive sample rate adjust mode, respectively, and counts sample numbers for one step. Here, we set the constant sample rate for capturing sensor data 20 times each step throughout the experiment, and the adaptive sample rate mode for capturing sensor data (1) 5 times each step when the experimenter is in stable state, and (2) 20 times each step when the experimenter is in non-stable state. The experimental data show that the adaptive sample rate adjustment mode reduces the energy consumption by 52 % in comparison with the constant sample mode, as shown in Fig. 13b.

### 5 Related works

Indoor pedestrian positioning and tracking systems are poised to serve as the foundation for context-aware services, and there exist many such commercially available indoor positioning and tracking technologies [16–18], classified in the following major categories: Fingerprint-based indoor localization techniques have been one of the most popular approaches to indoor localization and pedestrian tracking [19]. This approach, that does not require any hardware deployment, has been to leverage already available wireless signals (e.g., WiFi, cellular) to profile a location, usually in the form of received signal strength indicator (RSSI) values. Of all fingerprint-based indoor localization techniques, WiFi-based techniques are primarily used due to the broad availability of WiFi infrastructure [17, 20, 21]. However, the operating frequency range of WiFi signals makes them susceptible to human presence and orientation as well as to the presence of small objects in a room. Moreover, as this requires information about the AP positions, and the propagation model can vary significantly indoors, the accuracy of the WiFi triangulation can be uneven. Thus, it exhibits several limitations when considering indoor environments where a person needs to be localized at the meter level.

The most popular and inexpensive technology for indoor pedestrian tracking is to employ inertial sensors [22]. The inertial sensor-based method works as a stand-alone method without any infrastructure requirement. In [23], Adaptive Kalman filters and activity-based map matching are utilized to detect step heading. However, errors accumulate quickly as walking distance increases. Li et al. [7] proposed a reliable and accurate indoor localization method using phone inertial sensors. However, they have not yet solved the problem of direction error, for which magnetic interference and body swing are the two major causes. To compensate for inaccuracies in heading estimation, Park et al. presented a pedestrian tracking system [24], which can eliminate accumulative errors in indoor corridor environments that are laid out in a perpendicular design. This setup has the obvious limitations that it is only useful in some specific indoor corridor environments and cannot adapt to a variety of randomly sized indoor spaces. Many other attempts have been to solve the problem with smartphone. But, these solutions make certain assumptions. In [25], SparseTrack uses a digital compass and an accelerometer in a smartphone to track pedestrian location and correct the location in sparse indoor environments. However, SparseTrack relies on an additional ultrasonic sensor, which is sparsely distributed, to adjust the current location directed by smartphones. In Lee et al. [26], proposed a method to estimate the orientation based on acceleration signals. But, it assumes that the initial orientation of the phone is known. To improve tracking accuracy, Footpath [27] matches the detected steps onto the expected route using sequence alignment algorithms from the field of bioinformatics, where an accurate indoor map is assumed but hard to get in some old buildings actually.

## 6 Conclusions

This paper presents a HMM-based pedestrian tracking system, called WTrack, using only geomagnetic sensors and acceleration sensors in smartphones for various indoor environments. Firstly, WTrack defines walk pattern for indoor pedestrians and models it with HMM. With the pre-defined fine-grained walk pattern, we developed HMM-based walk pattern recognition to track indoor pedestrians, which is robust to body swing of natural walking. Outlier and bad zone of the trace can be recognized and calibrated. Meanwhile, an effective algorithm is proposed to recognize and calibrate the geomagnetic disturbances caused by objects. To capture accurate sensor data with minimum energy consumption, we propose an adaptive sampling mode. WTrack is capable of eliminating cumulative locating errors caused by noisy inertial sensors without any additional infrastructure or extra sensors and provides

meter-level positioning accuracy. The experimental results showed WTrack effectively reduces power consumption by adaptive sample rate adjustment up to 52 % and significantly improve the positioning accuracy up to 92.5 %.

**Acknowledgments** This work was partially supported by the National Key Basic Research Program of China “973 Project” (Grant No. 2011CB707106), the National High-Tech Research and Development Program of China “863 Project” (Grant No. 2013AA122301), the Program for Changjiang Scholars and Innovative Research Team in University (Grant No. IRT1278), the National Natural Science Foundation of China NSFC (Grant No. F020201, 61070013, 61250110541, U1135005, 61303212), “Hundred Talents Recruitment Program” of Global Experts of Hubei, and the US National Science Foundation (Grant No. CNS-1136027).

## References

1. Zhang B, Chen K, Cheng Y et al (2012) Location-log: bringing online shopping benefits to the physical world with magnetic-based proximity detection. In: Proceedings of ACM/IEEE IPSN, pp 1–5
2. Hong F et al (2012) Pocket mattering: indoor pedestrian tracking with commercial smartphone. In: International conference on indoor positioning and indoor navigation, vol 13
3. Jin Y et al (2011) A robust dead-reckoning pedestrian tracking system with low cost sensors. In: Proceedings of IEEE PerCom, pp 222–230
4. Bahl P, Padmanabhan VN (2000) RADAR: an in-building RF-based user location and tracking system. In: Proceedings of IEEE PerCom, pp 775–784
5. Yang Z, Wu C, Liu Y (2005) Locating in fingerprint space: wireless indoor localization with little human intervention. In: Proceedings of ACM MobiCom, pp 269–280
6. Rai A et al (2013) Zee: zero-effort crowdsourcing for indoor localization. In: Proceedings of ACM MobiCom, pp 293–304
7. Li F, Zhao C et al (2012) A reliable and accurate indoor localization method using phone inertial sensors. In: Proceedings of ACM UbiComp, pp 421–430
8. Lee S et al (2013) Smartphone-based indoor pedestrian tracking using geo-magnetic observations. In: Mobile Information Systems, pp 123–137
9. Harle R (2013) A survey of indoor inertial positioning systems for pedestrians. IEEE Commun Surv Tutor 15(3):1281–1293
10. Faulkner WT et al (2010) GPS-denied pedestrian tracking in indoor environments using an imu and magnetic compass. In: Proceedings of ITM, pp 198–204
11. Constandache I et al (2010) Towards mobile phone localization without war-driving. In: Proceedings of IEEE INFOCOM, pp 1–9
12. Steinhoff U, Schiele B (2010) Dead reckoning from the pocketan experimental study. In: Proceedings of IEEE PerCom, pp 162–170
13. Woodman O, Harle R (2008) Pedestrian localization for indoor environments. In: Proceedings of ACM UbiComp, pp 114–123
14. Hsiao R, Schultz T (2011) Generalized Baum-Welch algorithm and its implication to a new extended Baum-Welch algorithm. In: Proceedings of INTERSPEECH, pp 773–776
15. Huang Z, Chang Y, Long B, Crespo JF, Dong A, Keerthi S, Wu SL (2012) Iterative Viterbi A\* algorithm for k-best sequential decoding. In: Proceedings of 50th annual meeting of the association for computational linguistics (ACL), pp 611–619
16. Chung J, Donahoe M, Schmandt C, Kim JJ, Razavai P, Wiseman M (2011) Indoor location sensing using geo-magnetism. In: Proceedings of ACM MobiSys, pp 141–154

17. Evennou F, Marx F (2006) Advanced integration of WiFi and inertial navigation systems for indoor mobile positioning. *EURASIP J Appl Sig Process* 2006:164
18. Guo J et al (2013) Square-root unscented Kalman filtering-based localization and tracking in the internet of things. *Pers Ubiquit Comput*. doi:[10.1007/s00779-013-0713-8](https://doi.org/10.1007/s00779-013-0713-8)
19. Robertson P, Angermann M (2009) Simultaneous localization and mapping for pedestrians using only foot-mounted inertial sensors. In: *Proceedings of ACM UbiComp*, pp 93–96
20. Youssef M, Agrawala AK (2005) The Horus WLAN location determination system. In: *Proceedings of ACM MobiSys*, pp 205–218
21. Shen G et al (2013) Walkie-Markie: indoor pathway mapping made easy. In: *Proceedings of USENIX NSDI*, pp 85–98
22. Feliz R et al (2009) Pedestrian tracking using inertial sensors. *J Phys Agents* 3(1):35–42
23. Gusenbauer D et al (2010) Self-contained indoor positioning on off-the-shelf mobile devices. In: *International conference on indoor positioning and indoor navigation*, pp 1–9
24. Park K et al (2013) Smartphone-based pedestrian tracking in indoor corridor environments. *Pers Ubiquit Comput* 17(2):359–370
25. Jin Y et al (2013) A robust indoor pedestrian tracking system with sparse infrastructure support. *IEEE Trans Mob Comput* 12:1392–1403
26. Lee W, Jung P, Song H (2013) Hybrid indoor location tracking for pedestrian using a smartphone. *Robot Intell Tech Appl* 208:431–440
27. Link J, Smith P, Viol N et al (2011) Footpath: accurate map-based indoor navigation using smartphones. In: *International conference on indoor positioning and indoor navigation*, pp 1–8